Aerosol Science and Technology

ISSN: 0278-6826 (Print) 1521-7388 (Online) Journal homepage: http://www.tandfonline.com/loi/uast20

# Experimental Study of Particle Deposition in Bends of Circular Cross Section

David Y. H. Pui , Francisco Romay-Novas & Benjamin Y. H. Liu

**To cite this article:** David Y. H. Pui , Francisco Romay-Novas & Benjamin Y. H. Liu (1987) Experimental Study of Particle Deposition in Bends of Circular Cross Section, Aerosol Science and Technology, 7:3, 301-315, DOI: 10.1080/02786828708959166

**To link to this article:** http://dx.doi.org/10.1080/02786828708959166

Published online: 07 Jun 2007.

# Experimental Study of Particle Deposition in Bends of Circular Cross Section

David Y. H. Pui, Francisco Romay-Novas, and Benjamin Y. H. Liu
*Particle Technology Laboratory, Mechanical Engineering Department, University of Minnesota, Minneapolis. MN 55455*



**The deposition efficiency of liquid particles in tube bends of circular cross section has been measured for flow Reynolds numbers of 100, 1000, 6000, and 10,000. The particle Reynolds number, $Re_p$, was in the range 0.6–3.9 for the laminar flow cases (i.e., $Re = 100$ and 1000), whereas for the turbulent flow cases (i.e., $Re = 6000$ and 10,000) $Re_p$ was in the range 1.3–12.7. Bends constructed of stainless steel and glass tubes of different diameters were used. The experiments were performed using monodisperse aerosols generated by the vibrating orifice aerosol generator. The results were in good agreement with the theory of Cheng and Wang for $Re = 1000$, but differed from theory for $Re = 100$. For the turbulent cases, no dependence was found on the flow Reynolds number and an exponential curve of deposition efficiency versus Stokes number was fitted to the experimental results. A theoretical justification of the form of the curve is given in the paper.**

## NOMENCLATURE

| | |
|---|---|
| $A$ | Deposition area of the bend |
| $a_t$ | Tube radius |
| $C$ | Slip correction factor |
| $C_1$ | Volumetric concentration |
| $De = \frac{Re}{\sqrt{R_0}}$ | Dean number |
| $D_p$ | Particle diameter |
| $f$ | Frequency |
| $F$ | Area factor |
| $K = F\pi$ | |
| $M$ | Mass |
| $N$ | Number concentration |
| $N_R = \frac{D_p}{2a_t}$ | Interception parameter |
| $P$ | Penetration |
| $Q$ | Aerosol flow rate |
| $Q_1$ | Liquid flow rate |
| $r$ | Radial polar coordinate in $x$–$y$ plane |
| $R_1$ | Inner radius of the bend |
| $R_2$ | Outer radius of the bend |
| $R_b$ | Radius of curvature of the bend |
| $R_0 = \frac{R_b}{a_t}$ | Curvature ratio |
| $Re = \frac{2a_tU_0}{\nu}$ | Flow Reynolds number |
| $Re_p = \frac{D_pU_0}{\nu}$ | Particle Reynolds number |
| $St = \frac{C\rho_pD_p^2U_0}{18\mu a_t}$ | Stokes number |
| $t = \frac{TU_0}{a_t}$ | Dimensionless time |
| $T$ | Time |
| $U = \frac{\bar{U}}{U_0}$ | Dimensionless fluid velocity |
| $\bar{U}$ | Fluid velocity vector |
| $U_0$ | Mean axial fluid velocity |
| $u_y$ | $y$-component of $\bar{U}$ |
| $v_p$ | Particle deposition velocity |
| $X = \frac{\bar{X}}{a_t}$ | Dimensionless particle position |

Aerosol Science and Technology 7:301–315 (1987)


0278-6826/87/$3.50

| | | | |
|---|---|---|---|
| $\overline{X}$ | Particle position vector | $\nu = \frac{\mu}{\rho}$ | Kinematic viscosity of the fluid |
| $x_{om}(z)$ | $x$-coordinate of the starting point of the limiting trajectory | $\rho$ | Density of the fluid |
| | | $\rho_p$ | Density of the particle |
| $x, y, z$ | Cartesian coordinates | $\tau = \frac{\rho_p D_p^2 C}{18\mu}$ | Particle relaxation time |
| $\eta$ | Deposition efficiency | $\Theta$ | Angular polar coordinate in $x$–$y$ plane |
| $\mu$ | Absolute viscosity of the fluid | | |



## INTRODUCTION

Inertial deposition of aerosol particles in bends is of importance in many practical problems. This mechanism must be considered when determining particle losses in aerosol sampling and transport systems. Inertial impaction is also an important mechanism of particle deposition in the human airways, which can be modeled by bifurcations and bends.

The impetus for the present study came from our interest in understanding the mechanics of aerosol sampling from high purity gas streams (Pui et al., 1986). High purity gases used in semiconductor manufacturing are usually transported in pipes under high pressure and high velocity conditions. In order to detect particulate contaminants in the gas, a representative aerosol sample must be extracted and delivered to the particle detector via a sampling tube for counting and sizing of the particles. To design a sampling system of high efficiency successfully, it is necessary to understand the various particle loss mechanisms in the system. The inertial deposition of aerosol particles in bends is one such mechanism we wish to study.

Even though the problem has been studied both theoretically and experimentally by a number of investigators, it is still unclear at present as to the applicable theory for the different flow regimes. The complexity of the flow field (three dimensional with strong secondary motion) makes it very difficult to calculate the particle trajectories and the deposition efficiency, which is defined as the fraction of particles deposited in the bend. The available experimental data are not sufficiently accurate to select definitively the applicable theory.

Several theoretical calculations have been made using different flow fields. Landahl and Herrmann (1949) assumed a parabolic flow without secondary motion. Hacker et al. (1953) used a potential flow to solve the problem. Yeh (1974) derived a formula to calculate the deposition efficiency using a laminar plug flow. Cheng and Wang (1975) developed a more complex solution and assumed a forced vortex flow, with the axis at the center of curvature of the bend, and neglected the existence of secondary flows. Crane and Evans (1977) were the first investigators that included in their calculations the effect of the secondary motion and drag force in ultrastokesian regime at high Reynolds number. However, their results do not differ very much from those obtained by Cheng and Wang (1975). Some years later, Cheng and Wang (1981) developed a new theory using a three-dimensional developed laminar flow model (Mori and Nakayama, 1965) to calculate the deposition efficiency in bends of circular cross section. Their calculation includes the effect of the secondary flow, and it is restricted to the Stokesian regime.

Experimental data of particle deposition in bends are very few. Landahl and Herrmann (1949) performed some experiments at Reynolds number of 3144 and 6270 for tube bends of curvature ratios—the ratio

of the bend curvature radius to the tube radius—of 5 and 8. Johnston and co-workers (1973, 1977) published a set of experimental results for Reynolds number in the range 311–2,071 and curvature ratio in the range 5–30. The results of these experiments showed the weak dependence of the curvature ratio on the deposition efficiency (a fact that is not obvious) and the strong dependence of the flow Reynolds number on the same parameter. Unfortunately, the experiments were not performed at constant flow Reynolds number, and they are not sufficiently complete to show definitively which is the best theory to apply.

In the present study, a series of experiments was performed using the latest aerosol instrumentations and experimental techniques. A vibrating orifice generator was used to produce monodisperse test aerosols and a sensitive fluorometric analysis technique was used to determine the deposition pattern and deposition efficiency of particles in bends. The results obtained are used to compare with the available theories, in particular, the latest theories of Cheng and Wang (1975, 1981), which are considered to be the most rigorous among the available theories.

## DEFINITION OF THE PROBLEM

When an aerosol stream is forced to have a change in direction, such as in a bend, large particles of high inertia are unable to follow the flow streamlines. These particles can collide with the walls and be removed from the suspending gas, depending on the initial particle position at the bend inlet and other parameters such as Stokes number and flow Reynolds number. On the other hand, small particles with low inertia can follow the streamlines closely and penetrate through the bend. By using monodisperse aerosols of different particle sizes and varying the flow velocity in the bend, it is possible to obtain efficiency curves for different conditions.

To treat this problem in a general way, it is convenient to use dimensionless parameters. Particle deposition in bends of circular cross section depends on five dimensionless groups as discussed in the paper by Cheng and Wang (1981): Stokes number ($St = C\rho_p D_p U_0^2/18\mu a_t$), particle Reynolds number ($Re_p = D_p U_0/\nu$), interception parameter ($N_R = D_p/2a_t$), flow Reynolds number ($Re = 2a_t U_0/\nu$), and curvature ratio ($R_0 = R_b/a_t$), where $C$ is the slip correction factor, $\rho_p$ the particle density, $D_p$ the particle diameter, $U_0$ the mean axial velocity in the bend, $\mu$ the fluid viscosity, $a_t$ the tube radius, $\nu$ the fluid kinematic viscosity, and $R_b$ the radius of curvature of the bend.

The most important parameters are the Stokes number and the flow Reynolds number if particle motion is in the Stokesian regime ($Re_p \leq 1$). The interception parameter can be neglected because the particle diameter is usually several orders of magnitude less than the tube diameter. The effect of the curvature ratio has been shown to be insignificant, both theoretically and experimentally for $5 \leq R_0 \leq 30$.

For a given tube diameter and flow Reynolds number, the Stokes number can be changed experimentally by using different particle sizes. However, the particle Reynolds number is proportional to the particle size and cannot be kept constant for a set of experiments. If the particle Reynolds number is low enough, the results can be compared with the existing theories, which usually consider particle motion to be in the Stokesian regime.

Our experiments were performed for flow Reynolds number of 100, 1000, 6000, and 10,000, with bends of stainless steel and glass of internal diameters of 0.93, 5.03, 8.51, and 3.95 mm. The Stokes number was varied from 0.1 to 1.4 for each set of experiments. The particle Reynolds number was in the range 0.6–3.9 for the laminar flow cases and in the range 1.3–12.7 for the turbulent flow cases.

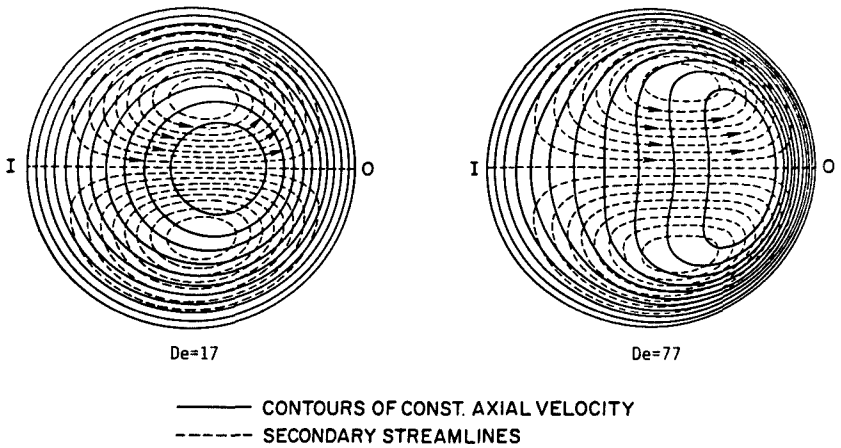


**FIGURE 1.** Secondary streamlines and axial velocity contours at low and intermediate Dean numbers (McConalogue and Srivastava, 1968).



## FLOW FIELD IN A BEND OF CIRCULAR CROSS SECTION

The flow field in bends of circular cross section depends only on the Dean number for bends of curvature ratio greater than five. The Dean number is defined as the flow Reynolds number divided by the square root of the curvature ratio ($De = Re/\sqrt{R_0}$). It represents the ratio of the square root of the product of centrifugal and inertial forces to the viscous forces (i.e., $De \alpha [\rho^2 U_0^2 / R_b]^{1/2}/\mu$). *De* plays the role of the "Reynolds number" of the flow in a curved pipe.

Researchers have defined three different flow regimes for the flow around circular bends. For small Dean number ($De \leq 17$), a pair of counterrotating helical vortices, placed symmetrically with respect to the plane of symmetry (see Figure 1) are formed because of the centrifugally induced pressure gradient that drives the slower moving fluid near the wall inward, while the faster moving fluid in the core is swept outward. The position of the maximum axial velocity moves toward the outer bend. The flow is more stable than in straight tubes (critical Reynolds number around 5000 for $R_0 = 31.9$) because of the stabilizing effect produced by the curvature.

For intermediate Dean number ($17 \leq De \leq 370$), the flow pattern is the same as before but with the peak velocity closer to the outer bend and a distortion of the secondary streamlines (a secondary boundary layer develop on the wall) (see Figure 1). In this regime, especially as the Dean number gets larger, the structure of the flow is characterized by an inviscid rotational core surrounded by a thin boundary layer. The flow is considered laminar at least for small and intermediate Dean number ($De \leq 370$).

For large Dean number ($De > 370$) the centrifugal force leads to an increase in axial velocity and to more fluid being drawn into the boundary layer near the outer bend. The secondary boundary layers adjust by thinning near the outer bend and thickening near the inner bend. The two vortices are skewed (see Figure 2). It is believed that there is a point at which there appears flow separation due to the thickening effect of the secondary boundary layer. There is no analytical model to describe accurately the flow field in this large Dean number range. Experimental results (Sparrow and Chrysler, 1986) have shown that the flow in a finite bend at high Reynolds number is almost always a developing flow. This fact further complicates the analytical solution of the problem for the turbulent case.

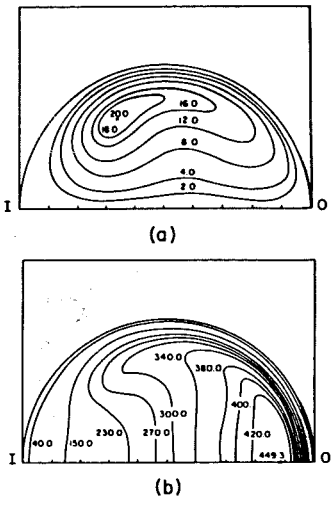


**FIGURE 2.** (a) Secondary streamlines and (b) axial velocity contours at large Dean number, $De = 370$ (Collins and Dennis, 1975).

## PARTICLE TRAJECTORY AND DEPOSITION EFFICIENCY

A theoretical calculation of the deposition efficiency requires the solution of the three-dimensional equations of particle motion. Neglecting gravitational and electrostatic forces and assuming particle motion to be in the Stokesian regime (i.e., drag force follows the Stokes law) the equation of motion assumes the following dimensionless form:

$$\frac{d^2X}{dt^2} = \frac{1}{St}\left[U - \frac{dX}{dt}\right], \tag{1}$$

where $X = \bar{X}/a_t$ is the position vector of a particle divided by the tube radius, $U = \bar{U}/U_0$ is the fluid velocity vector divided by the mean axial tube velocity, and $t = U_0 T/a_t$ is dimensionless time.

The initial conditions for solving Eq. (1) are given by (see Figure 3):

$$x = x_0;$$
$$y = 0;$$
$$z = z_0;$$
$$\frac{dX}{dt} = U. \tag{2}$$

With a suitable flow field, Eq. (1) can be solved numerically using the fourth-order Runge–Kutta method [see Cheng (1976)].

By solving the particle motion equation for a set of data ($St$, $Re$, and $R_0$) with different initial positions, the $x$-coordinate of the starting point of the limiting trajectory (trajectory that separates the penetrating and deposited particles) at a given $z$ can be found. The deposition efficiency can then be calculated from:

$$\eta = \frac{\int_0^{a_t}\int_{x_{om}}^{R_2} u_y \, dx \, dz}{\int_0^{a_t}\int_{R_1}^{R_2} u_y \, dx \, dz}, \tag{3}$$

where $x_{om}(z)$ is the $x$-coordinate of the starting point of the limiting trajectory. It is important to note that the above definition of deposition efficiency takes into account only the fraction of particles deposited in the bend and does not include those that are deposited after the exit plane of the bend.

Figure 4 presents the most important theoretical calculations of deposition efficiency versus Stokes number using different flow fields.

## EXPERIMENTAL

### System Setup

Figure 5 is a schematic diagram of the system used. The test aerosol was generated by the vibrating orifice aerosol generator (Model 3450, TSI Inc., St. Paul, MN) and divided in two streams at the exit of the neutralizer. The flow required for the bend was regulated using a valve downstream of the filter holder. The excess aerosol was filtered before being exhausted to the laboratory.

Bends of stainless steel and glass were built using a standard tube bender ($R_0 = 5.7$). For $Re = 100$, a glass tube bend of 0.93-mm i.d. was used. For $Re = 1000$, 6000, and 10,000, metallic and glass bends of 5.03, 8.51, and 3.95-mm i.d. were used. The bends

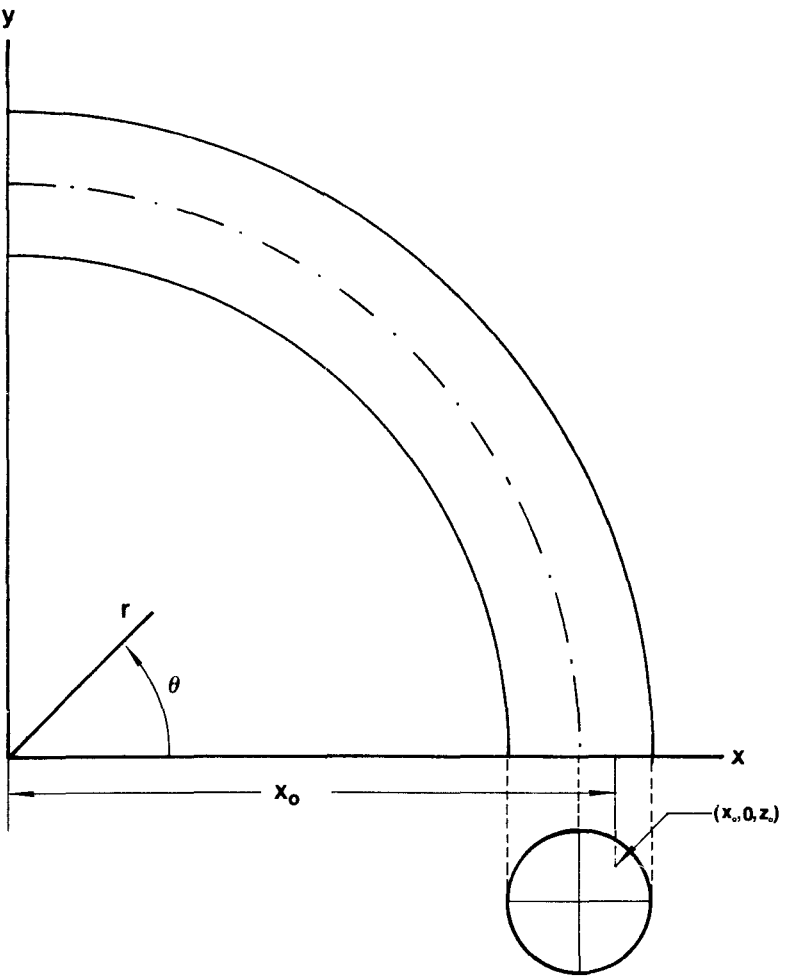


**FIGURE 3.** Bend in rectangular coordinates with particle at initial position.

were set up with an horizontal inlet section for all the cases except for the case $Re = 100$, where a vertical inlet section was used. With the horizontal inlet the particle concentration profile at the entrance to the bend was not completely uniform, as there was some particle settling in the horizontal inlet section. For the case $Re = 100$, the settling became excessive and nonrepeatable results were obtained. All the bends had an inlet section sufficiently long so that a fully developed flow profile was obtained prior to the bend.

After the bend a filter holder containing a high efficiency particulate filter (glass fiber filter type A/E from Gelman Sciences Inc., Ann Arbor, MI or membrane filter GSWP01300 from Millipore Co., Bedford, MA) was used to collect all the particles penetrating through the tube sections. Downstream of the filter, the flow meter, the regulating valve, and the vacuum pump were installed.

### Aerosol Generation

The test aerosol was generated using the vibrating orifice aerosol generator (Berglund and Liu, 1973), which can generate highly

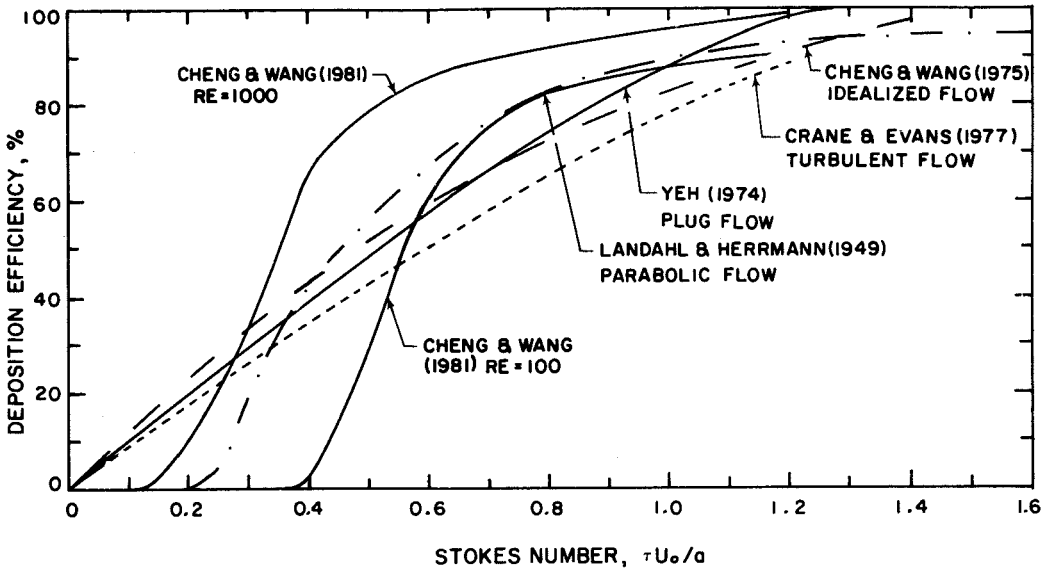


**FIGURE 4.** Theoretical efficiency curves for particle deposition in bends.

monodisperse liquid and solid aerosols of different sizes. The uniform droplets are generated when the solution is forced through a small orifice with a syringe pump at a known rate, and the liquid jet is broken up into droplets by a piezoelectric ceramic.

The liquid solution consisted of oleic acid dissolved in special denatured alcohol to which a small quantity of uranine (1 g/liter)

**FIGURE 5.** Experimental system.

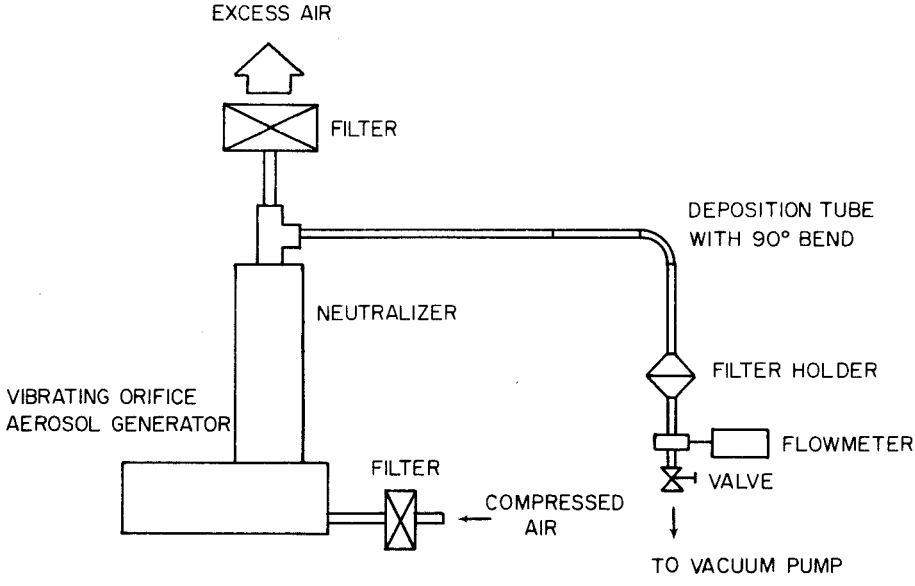

had been added. The uranine was used as a fluorescent tracer for quantitative analysis of the deposited particles. The solution of known concentration was sprayed through the vibrating orifice. After the solvent (denatured alcohol) is evaporated from the solution droplets, the desired uranine-tagged oleic acid aerosol is obtained. The diameter of the generated particles can be calculated very accurately (2% or better) from the operating conditions with the formula:

$$D_p = [6Q_1C_1/\pi f]^{1/3}, \quad (4)$$

where $C_1$ is the volumetric concentration of the nonvolatile solute (oleic acid and uranine) in the solution, $Q_1$ is the volumetric liquid flow rate fed to the generator, and $f$ is the vibrating frequency of the orifice.

The liquid aerosol generated was neutralized in the generator by a 10 mCi krypton-85 radioactive source to reduce the particle electrostatic charge to a low level, so that deposition was not affected by electrostatic effects.

Because liquid aerosols were used, it was assumed that particles would adhere to the tube surface upon contact. Particle bounce from the bend walls was not considered to be a problem.

## Flow Measurement

For low flows ($Re = 100$), a linear flow meter previously calibrated with a bubble flow meter was used. For higher flows ($Re = 1000$ and higher), a hot film flow transducer (TSI Inc., St. Paul, MN) was used. The uncertainty of the flow measurement was estimated to be 5% for the linear flow meter and 3% for the hot film transducer.

## Experimental Procedure

The procedure of each experimental run consisted of first adjusting the flow to the required value and then connecting the aerosol generated under stable conditions to the system. The sampling time was varied from 5 to 30 min depending on the particle size, the flow Reynolds number, and the tube diameter.

The mass of uranine collected on the filter was measured by removing the filter from the filter holder and immersing the entire filter in 25 or 50 ml of 0.001 N solution of NaOH in distilled water in a glass beaker. The concentration of uranine in the washing solution was then measured with a calibrated fluorometer (Fluoro-colorimeter of American Instrument Co., Silver Spring, MD).

The uranine deposited in the probe walls for all the experimental runs, except for the 0.93-mm-i.d. bend, was removed as follows: the probe was subdivided into five sections (Figure 6). Sections 1, 2, 4, and 5 were wiped by means of cotton swabs wetted in washing solution and then letting the uranine in the swabs dissolve in 25 ml of washing solution in glass beakers. Section 3 (bend) was then rinsed with 25 or 50 ml of washing solution. After 30 min, the concentration of the solution of each section was measured. It is important to remark that the above proce-

**FIGURE 6.** Details of deposition tube with bend for deposition experiments at $Re = 1000$, 6000, and 10,000.

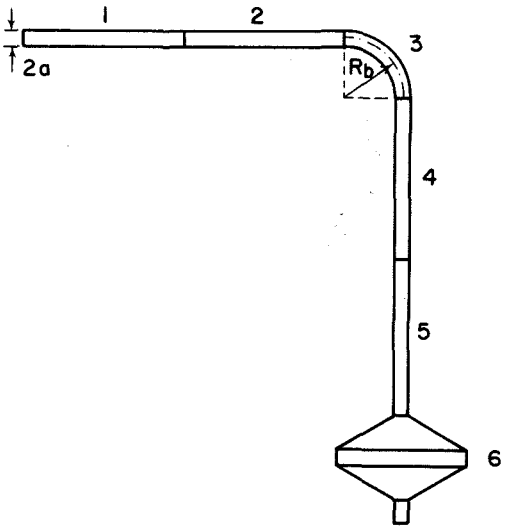

dures was more accurate for the glass bend than for the stainless-steel bends, because it was possible to wipe the sections while looking through the transparent walls of the bend. For the bend of 0.93-mm i.d. another procedure was used. For this case the probe was subdivided into three sections. First, the external surface of the probe was cleaned with distilled water. Then, the inlet and exit straight sections were immersed, respectively, into culture tubes with 3.8 ml of washing solution. After letting the tube section dry, the uranine in the bend was collected by injecting 5 ml of washing solution through the bend using a graduated syringe. Finally, the concentration of uranine for each solution was measured. For this case the filter was immersed in 5 ml of washing solution in a glass beaker.

The techniques described above were found to give very repeatable results. During the course of the experiments, some runs were repeated on different days, and the difference observed between them was less than 3%.

The uncertainty in the calculation of the experimental Stokes number was estimated to be 5% for all the experimental runs, except for the case $Re = 100$ where the estimated uncertainty was 8%. The uncertainty in the experimental deposition efficiency was estimated to be 3%.

## RESULTS AND COMPARISON WITH THEORIES

Table 1 shows the results for a typical run. The collection efficiency of the bend is calculated by dividing the mass of uranine collected in the bend by the total mass of uranine that entered the bend:

$$\eta = \frac{M_{\text{bend}}}{M_{\text{bend}} + M_{\text{after bend}}}. \tag{5}$$

Table 2 shows the summary of results for all the experimental runs for flow Reynolds number of 1000, 6000, 10,000, and 100.

Figure 7 shows the collection efficiency of the bend versus the Stokes number for the case $Re = 1{,}000$. The solid curve is the numerical curve calculated by Cheng and Wang (1981) for the same case. The data points taken with the glass tube are very close to the predicted curve. The other data points taken with the stainless steel bends are less close to the curve. The difference among data points with different tubes is attributed to experimental errors in the wiping procedure, especially with the stainless steel tube. However, we can conclude that the theory works very well for this particular Reynolds number. This is due to the fact that the Dean number during these experimental runs was 420, and the flow field equations used (Mori and Nakayama, 1965) by Cheng and Wang (1981) are applicable.

**TABLE 1.** Experimental Data for a Typical Run

| | | |
|---|---|---|
| Run No. 8 | | |
| Probe i.d. (mm): 3.95 | Curvature ratio: 5.7 | Material: glass |
| Flow rate ($cm^3/s$): 47.3 | Velocity (cm/s): 386 | Sampling time (min): 10 |
| Fluorometric analysis | | |
| Section | | Uranine deposition ($\mu g$) |
| 1 | | 0.0473 |
| 2 | | 0.0205 |
| 3 (bend) | | 1.19 |
| 4 | | 0.0090 |
| 5 | | 0.0239 |
| 6 (filter) | | 3.65 |
| Reynolds number: 1000 | | Particle diameter ($\mu m$): 7.20 |
| Stokes number: 0.28 | | Deposition efficiency: 0.245 |

**TABLE 2.** Summary of Experimental Results

| Run | Tube i.d. (mm) | Material | $R_0$ | $Re_p$ | $St$ | $\eta$ (%) |
|---|---|---|---|---|---|---|
| $Re = 1000$ | | | | | | |
| 1 | 5.03 | Stainless steel | 5.7 | 1.1 | 0.08 | 1.4 |
| 2 | 5.03 | Stainless steel | 5.7 | 1.6 | 0.21 | 26.4 |
| 3 | 5.03 | Stainless steel | 5.7 | 2.1 | 0.39 | 49.5 |
| 4 | 5.03 | Stainless steel | 5.7 | 2.8 | 0.65 | 88.5 |
| 5 | 5.03 | Stainless steel | 5.7 | 3.5 | 1.03 | 91.8 |
| 6 | 5.03 | Stainless steel | 5.7 | 3.9 | 1.26 | 94.0 |
| 7 | 3.95 | Glass | 5.7 | 1.4 | 0.17 | 5.3 |
| 8 | 3.95 | Glass | 5.7 | 1.8 | 0.28 | 24.5 |
| 9 | 3.95 | Glass | 5.7 | 2.0 | 0.33 | 37.7 |
| 10 | 3.95 | Glass | 5.7 | 2.1 | 0.37 | 63.2 |
| 11 | 3.95 | Glass | 5.7 | 2.3 | 0.44 | 74.6 |
| 12 | 3.95 | Glass | 5.7 | 2.6 | 0.57 | 84.9 |
| 13 | 3.95 | Glass | 5.7 | 2.9 | 0.70 | 93.7 |
| 14 | 3.95 | Glass | 5.7 | 3.3 | 0.90 | 94.8 |
| 15 | 3.95 | Glass | 5.7 | 3.7 | 1.12 | 96.9 |
| 16 | 3.95 | Glass | 5.7 | 3.9 | 1.24 | 94.2 |
| 17 | 8.51 | Stainless steel | 5.6 | 1.0 | 0.10 | 1.5 |
| 18 | 8.51 | Stainless steel | 5.6 | 1.4 | 0.17 | 22.7 |
| 19 | 8.51 | Stainless steel | 5.6 | 1.7 | 0.23 | 43.5 |
| 20 | 8.51 | Stainless steel | 5.6 | 2.1 | 0.36 | 53.0 |
| 21 | 8.51 | Stainless steel | 5.6 | 2.3 | 0.44 | 67.6 |
| $Re = 6000$ | | | | | | |
| 22 | 5.03 | Stainless steel | 5.7 | 1.3 | 0.03 | 6.1 |
| 23 | 5.03 | Stainless steel | 5.7 | 2.9 | 0.13 | 13.4 |
| 24 | 5.03 | Stainless steel | 5.7 | 3.5 | 0.19 | 29.6 |
| 25 | 5.03 | Stainless steel | 5.7 | 4.9 | 0.36 | 55.0 |
| 26 | 5.03 | Stainless steel | 5.7 | 6.3 | 0.60 | 76.0 |
| 27 | 5.03 | Stainless steel | 5.7 | 7.0 | 0.72 | 80.6 |
| 28 | 5.03 | Stainless steel | 5.7 | 8.3 | 1.00 | 88.4 |
| $Re = 10{,}000$ | | | | | | |
| 29 | 8.51 | Stainless steel | 5.6 | 5.6 | 0.27 | 48.4 |
| 30 | 8.51 | Stainless steel | 5.6 | 5.8 | 0.29 | 50.3 |
| 31 | 8.51 | Stainless steel | 5.6 | 7.3 | 0.46 | 65.6 |
| 32 | 8.51 | Stainless steel | 5.6 | 9.5 | 0.75 | 82.7 |
| 33 | 5.03 | Stainless steel | 5.7 | 9.9 | 0.84 | 83.1 |
| 34 | 5.03 | Stainless steel | 5.7 | 12.0 | 1.22 | 94.0 |
| 35 | 5.03 | Stainless steel | 5.7 | 12.7 | 1.35 | 94.8 |
| $Re = 100$ | | | | | | |
| 36 | 0.93 | Glass | 7 | 0.6 | 0.28 | 3.0 |
| 37 | 0.93 | Glass | 7 | 0.6 | 0.34 | 5.6 |
| 38 | 0.93 | Glass | 7 | 0.7 | 0.46 | 12.4 |
| 39 | 0.93 | Glass | 7 | 0.8 | 0.57 | 17.6 |
| 40 | 0.93 | Glass | 7 | 1.0 | 0.76 | 34.8 |
| 41 | 0.93 | Glass | 7 | 1.0 | 0.83 | 39.9 |
| 42 | 0.93 | Glass | 7 | 1.1 | 0.93 | 64.7 |
| 43 | 0.93 | Glass | 7 | 1.2 | 1.29 | 82.9 |
| 44 | 0.93 | Glass | 7 | 1.3 | 1.46 | 88.0 |

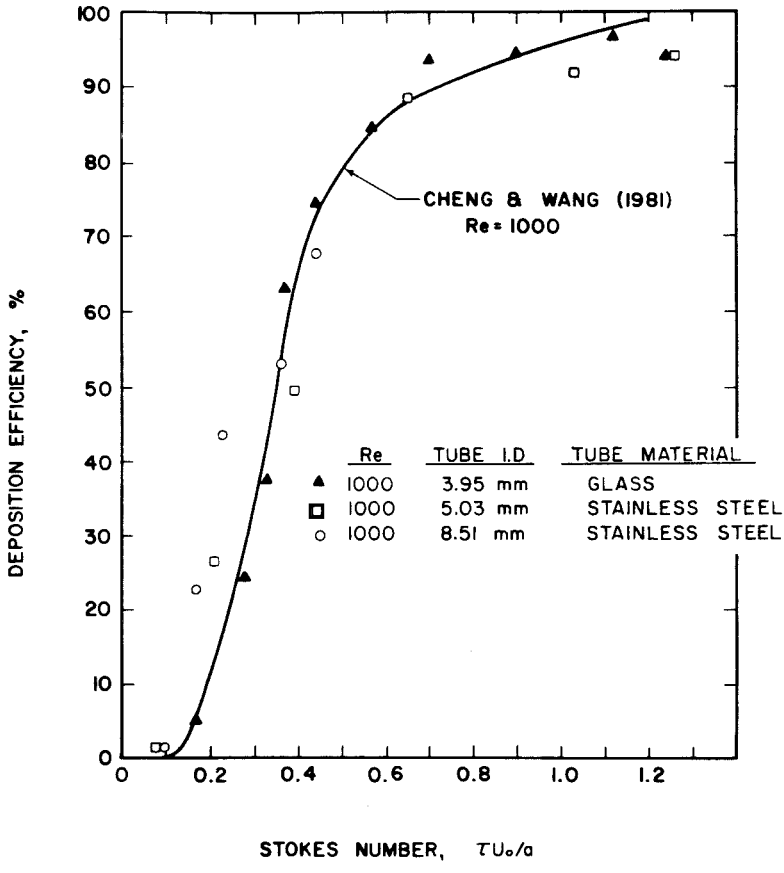


**FIGURE 7.** Particle deposition in bends at $Re = 1000$.

The experimental runs performed with the glass tube allowed us to study the deposition pattern of the particles in the bend. For large Stokes number, the outer bend was completely covered with a layer of particles. For medium Stokes numbers, the outer bend had a vertical stripe free of particles. This is due to the symmetrical counterrotating vortices that drive the particles to the inner bend. For low Stokes numbers, the zone free of particles is larger and more deposited particles can be seen in the inner bend. The different deposition patterns developed are a consequence of the particle inertia and secondary flow. As the particles become smaller, they can better follow the secondary flow in contrast to the case of large particles. These observations are a visual proof of the strong influence of the secondary flow in the particle trajectories and of the fact that particles deposit not only in the outer bend but also in the inner bend.

Figure 8 shows the collection efficiency data for the case of $Re = 100$. The solid curve is again the numerical prediction of Cheng and Wang (1981). For this low Reynolds number the predicted curve does not agree with the experimental results. This can be explained by observing that the Dean number for these experimental runs was very small (i.e., $De = 35$), and the flow field cannot be characterized by a boundary layer and a core region (Mori and Nakayama, 1965). Therefore, the solution given by Cheng and Wang (1981) does not apply. For laminar flows with low Dean's number, Dean's solution or numerical solutions can be used to

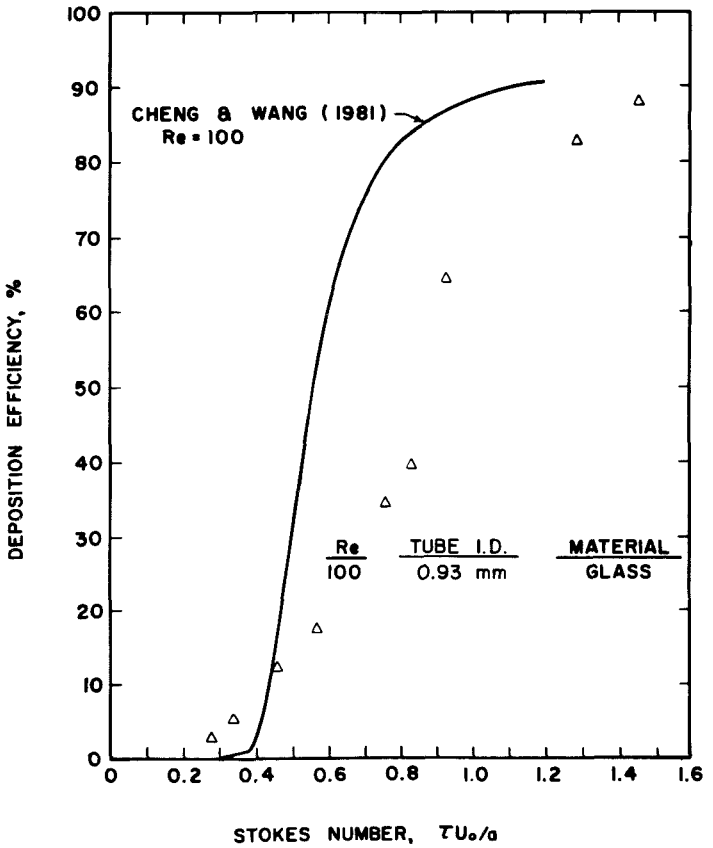


**FIGURE 8.** Particle deposition in bends at $Re = 100$.

obtain the deposition efficiency. By visual observation it was found that for this case there is significant deposition of particles in the last portion of the bend and right after the bend. This can be the explanation for the lower values of the deposition efficiency found experimentally.

In conclusion, we can say that in the laminar case the theory of Cheng and Wang is valid for laminar flows with intermediate and large Dean's number (flow Reynolds number not too low). For practical purposes, it would be useful to have more theoretical efficiency curves for other laminar flow Reynolds numbers (i.e., $Re = 2000$, 3000, 4000, and 5000). Unfortunately, this is not available at present.

Figure 9 shows the experimental data obtained for the turbulent flow regime ($Re =$ 6000 and 10,000). The deposition efficiency was found to be independent of the flow Reynolds number. The experimental efficiencies are clearly higher than those predicted by the idealized flow model of Cheng and Wang (1975). From the experimental data, a curve was fitted so that a simple formula can be used to calculate the particle losses in bends with turbulent flow. Figure 10 shows the aerosol penetration $P$ ($P = 1 - \eta$) versus the Stokes number plotted in a semilog scale. The data can be fitted by the straight line $\log P = -0.963\ St$ with a correlation coefficient of 0.995. Therefore, the deposition efficiency can be calculated by:

$$\eta = 1 - 10^{-0.963\ St}. \tag{6}$$

The exponential form of the curve can be explained using the turbulent mixing theory.

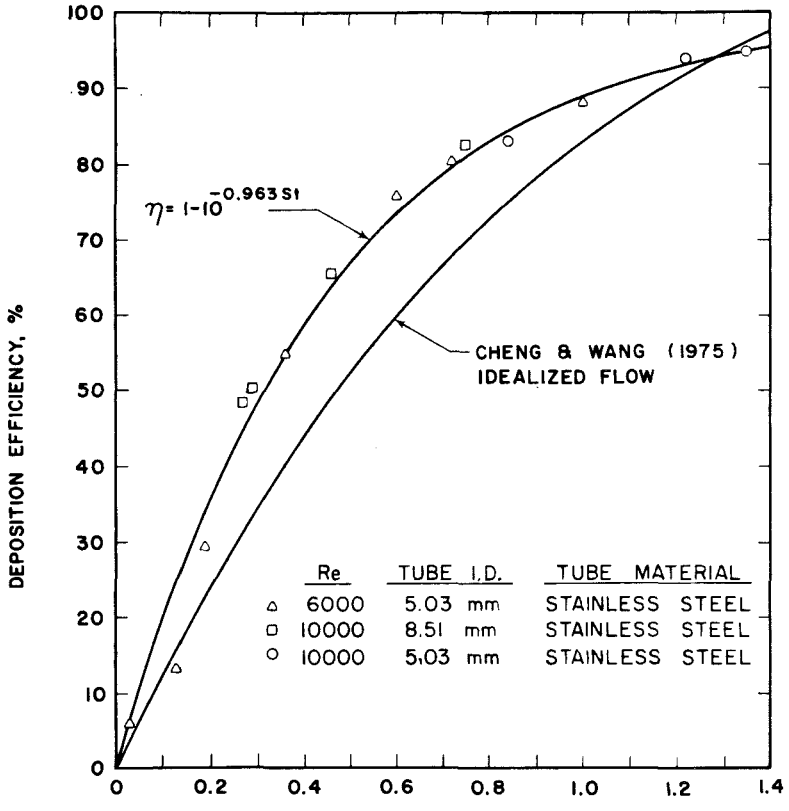


**FIGURE 9.** Particle deposition in bends: turbulent regime.

Consider for the moment a monodisperse aerosol flowing in a tube. Assume that the flow is turbulent and that particles deposit on the walls of the tube at a constant deposition velocity. The concentration in the stream is assumed to be constant due to the perfect turbulent mixing. If we select a differential control volume and make a mass balance, it follows that:

$$\frac{dN}{N} = -\frac{v_p\, dA}{Q}, \tag{7}$$

where $N$ is the number concentration, $v_p$ is the deposition velocity of the particles, $A$ is the deposition area, and $Q$ is the volumetric flow rate. By integrating Eq. (7), the total fractional penetration of the aerosol stream is then given by:

$$P = e^{-Av_p/Q}. \tag{8}$$

By applying the above theory to our system, a 90° bend of circular cross section, the deposition velocity, can be assumed to be given by:

$$v_p = \frac{\tau U_0^2}{R_b}, \tag{9}$$

where $\tau$ is the particle relaxation time, and the flow rate is calculated from:

$$Q = \pi a_t^2 U_0. \tag{10}$$

Therefore, Eq. (8) can be reduced to:

$$\ln P = -\frac{A}{R_b \pi a_t}(\tau U_0/a_t) = -KSt, \tag{11}$$

where $K = A/R_b \pi a_t$ and $St = \tau U_0/a_t$.

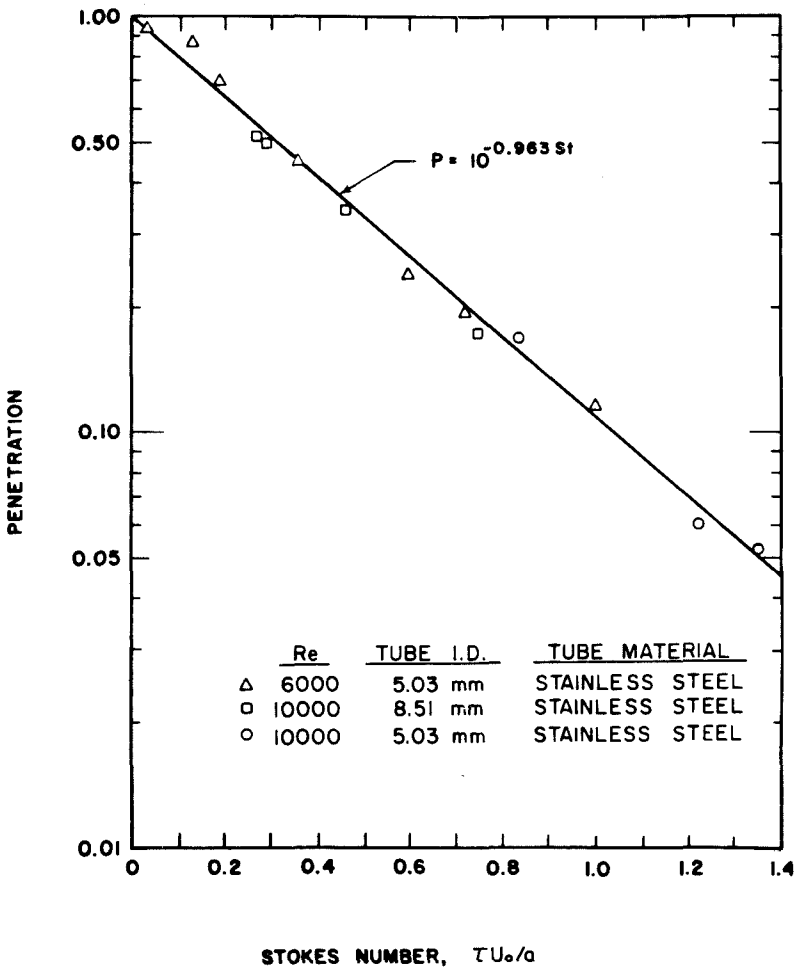


**FIGURE 10.** Particle penetration in bends: turbulent regime.

The deposition area is a fraction of the total internal area of the bend and is given by:

$$A = F\left[(\pi R_b/2)(2\pi a_t)\right] = F\left(\pi^2 R_b a_t\right), \tag{12}$$

where $F$ is an area factor less than one.

Substituting Eq. (12) into the expression for $K$, it follows that:

$$K = F\pi. \tag{13}$$

From the experimental correlation:

$$\ln P = -St(0.963 \ln 10). \tag{14}$$

From Eqs. (11), (13), and (14), $K = F\pi = 0.963 \ln 10$ and

$$F = 0.963 \ln 10/\pi = 0.706. \tag{15}$$

This result means that approximately 71% of the total internal area of the bend is the effective collecting surface of the bend. This can be explained because of the secondary motion, which allows particles to deposit in the outer and inner bend.

## APPLICATIONS

The experimental results obtained can be applied to the design of aerosol sampling systems with bends. For example, consider a sampling line of 2.5-cm i.d. with a standard 90° bend. The system draws 100 liters/min

of air, and we want to know what is the fractional penetration of 10-$\mu$m particles of unit density through the bend. The solution to this simple problem is given below.

Vol. flow rate: $Q = 100$ liters/min $= 1667$ cm$^3$/s.

Mean axial vel.: $U_0 = Q/\pi a_t^2 = 339.5$ cm/s.

Absolute viscosity of air: $\mu = 1.83 \times 10^{-4}$ $P$ (dyn-s/cm$^2$).

Kinematic viscosity of air: $\nu = 0.153$ $St$ (cm$^2$/s).

Flow Reynolds number: $Re = 2a_t U_0/\nu = 5{,}548$ (turbulent).

Stokes number: $St = C\rho_p D_p U_0^2/18\mu a_t = 0.082$.

Fractional penetration: $P = 10^{-0.963\ St} = 0.834$.

For the laminar cases, the curve of Cheng and Wang (1981) for $Re = 1000$ can be used if the actual Reynolds number is close to 1000. For other laminar flow Reynolds numbers, more curves using the theory of Cheng and Wang (1981) can be developed for $1000 \leq Re \leq 5000$. However, for very low Reynolds number a better theoretical prediction is needed.

From the results of these experiments, it can be concluded that for the turbulent regime the deposition efficiency approaches zero as the Stokes number goes to zero. The form of the deposition efficiency curve is exponential (i.e., $\eta = 1 - 10^{-0.963\ St}$) and independent of the flow Reynolds number. On the other hand, in the laminar regime the deposition efficiency approaches zero for finite Stokes numbers (i.e., $St = 0.1$ and 0.2 for $Re = 1000$ and 100, respectively). The form of the deposition efficiency curve is sigmoidal and highly dependent on the flow Reynolds number. These remarks imply that in order to have negligible particle losses in bends, the Stokes number should be kept small.

This research is supported by the Particulate Contamination Control Research Consortium at the University of Minnesota. Members of the Consortium include: Control Data Corporation, Donaldson Company, Inc., Liquid Air Corporation, Millipore Corporation, Texas Instruments, Inc., and TSI, Inc. The support of the Consortium is gratefully acknowledged.

## REFERENCES

Berger, S. A., Talbot, L., and Yao, L. S. (1983). *Annu. Rev. Fluid Mech.* 15:461–512.

Berglund, R. N., and Liu, B. Y. H. (1973). *Environ. Sci. Technol.* 7:147–153.

Cheng, Y. S. (1976). *Particle Deposition in Bends and Repeatedly Bifurcating Tubes.* Ph.D. Dissertation, Syracuse University, Syracuse, New York.

Cheng, Y. S., and Wang, C. S. (1975). *J. Aerosol Sci.* 6:139–145.

Cheng, Y. S., and Wang, C. S. (1981). *Atmos. Environ.* 15:301–306.

Collins, W. M., and Dennis, S. C. R. (1975). *Q. J. Mech. Appl. Math.* 28:133–156.

Crane, R. I., and Evans, R. L. (1977). *J. Aerosol Sci.* 8:161–170.

Hacker, P. T., Brun, R. J., and Boyd, B. (1953). *NACA Technical Note No. 2999.*

Johnston, J. R., and Muir, D. C. F. (1973). *J. Aerosol Sci.* 4:269–270.

Johnston, J. R., Isles, K. D., and Muir, D. C. F. (1977). In *Inhaled Particles* (W. H. Walton, ed.). Pergamon Press, Oxford, Vol. 4, pp. 61–72.

Landahl, H. D., and Herrmann, R. G. (1949). *J. Colloid Sci.* 4:103–136.

McConalogue, D. J., and Srivastava, R. S. (1968). *Proc. R. Soc. A.* 307:37, 53.

Mori, Y., and Nakayama, W. (1965). *Int. J. Heat Mass Transfer* 8:67–82.

Pui, D. Y. H., Kuehn, T. H., and Liu, B. Y. H. (1986). Presentation at the Second International Aerosol Conference, West Berlin, Germany, September 22–26, 1986.

Sparrow, E. M., and Chrysler, G. M. (1986). *ASME J. Heat Transfer*, 108:40–47.

Yeh, H. C. (1974). *Bull. Math. Biol.*, 36:105–116.

Yeh, H. C. (1976). *J. Aerosol Sci.* 7:275–276.

Received 14 October 1986; accepted February 1987